LUNDS UNIVERSITET

Bachelor's Thesis

The Spatial Properties of the Beam Profile of an OPCPA

Author:
Mattias Bengtsson

Supervisor:
Anne Harth

Abstract

OPCPA stands for optical parametric chirped-pulse amplification. It is a nonlinear method for amplifying broadband laser beams. The spatial properties of the output of the laser beam depends on the amplification method itself and the broadband configuration. The phase matching in this method causes the different wavelengths in the broadband to have different angular dispersions.

In order to investigate this, an imaging spectrometer was designed, built, and calibrated. A spectrometer is a tool used to measure the wavelengths of a light source. An imaging spectrometer can also measure the spatial information of the individual wavelengths in one direction from the light source. This information can be either the position and the width or the angular dispersion. The built imaging spectrometer observes the former.

In order to test the capacity of the spatial measurements of the imaging spectrometer, a prism wedge is placed in the beam path from the oscillator to give a known divergence to the individual wavelengths. After that, the spectrum from the OPCPA beam is recorded and discussed. The amplified beam is also rotated 90° to see the spatial properties in the other axis.

Contents

1 Introduction

Lasers have become a big part of our lives. In research they are used in novel experiments. This research often requires high intensities and good beam profiles. It is important to study the beam profiles of different amplification processes.

There are several ways to amplify laser beams. Optical parametric chirped-pulse amplification (OPCPA) is one of these. This amplification works by first stretching the short pulses in time to decrease the intensity. Then, the signal beam and the pump beam are propagated through a crystal with $\chi^{(2)}$ nonlinearity to increase the gain. The amplified beam is then compressed to short pulses increasing the intensity again.

The OPCPA used was VENTEON's VENTEON — PULSE : THREE system. This system is the first commercially available OPCPA system. Therefore, it is of importance to investigate this system, and in this thesis we focus on the beam profile.

An imaging spectrometer was made to investigate the spatial component of the beam of the OPCPA system. Due to the amplification process, the different wavelengths get different angular dispersions. A spectrometer measures the different wavelengths of a light source. The imaging spectrometer can also measure the widths, or spatial component, of the beam at different wavelengths.

In this report, a simulation of difference frequency generation of an OPA will be shown. Then, the set-up of the imaging spectrometer and its calibration will be presented. After that, the experimental set-ups and the results will be put forth and discussed. Finally, a conclusion will be presented with an outlook.

2 Theory

In order to understand the need for the imaging spectrometer, this section details the influence of the nonlinear processes of the OPCPA on the angular dispersion.

2.1 Nonlinearity

Linear optics can be described by

$$\tilde{P}(t) = \epsilon_0 \chi^{(1)} \tilde{E}(t)$$

where $\tilde{P}(t)$ is the induced polarization of the electric field $\tilde{E}(t)$, ϵ_0 is the free space permittivity constant, and $\chi^{(1)}$ is the linear susceptibility [1].

In nonlinear optics, this relation is modified into a power series

$$\tilde{P}(t) = \epsilon_0 \Big(\chi^{(1)} \tilde{E}(t) + \chi^{(2)} \tilde{E}^2(t) + \chi^{(3)} \tilde{E}^3(t) + \cdots \Big) \equiv \tilde{P}^{(1)}(t) + \tilde{P}^{(2)}(t) + \tilde{P}^{(3)}(t) + \cdots$$

where $\chi^{(2)}$ is the second-order nonlinear optical susceptibility, $\chi^{(3)}$ is the third-order nonlinear optical susceptibility, and so forth. The physical processes originating from the $\chi^{(2)}$ susceptibility are second-harmonic generation (SHG), difference frequency generation (DFG), and sum frequency generation (SFG). The $\chi^{(3)}$ susceptibility is responsible for third-harmonic generation (THG) and four-wave mixing (FWM).

In crystals that show inversion symmetry, $\chi^{(2)}$ susceptibility term cancels out. Therefore, optical parametric amplification (OPA) uses crystals that lack inversion symmetry, which allows parametric amplification. In this case, the signal beam and a pump beam of a shorter wavelength are directed through a crystal. Photons from the pump beam are changed equally into photons matching the signal beam and photons creating the idler beam. The energies of the created photons in the idler beam and the signal beam add up to the energy of the pump beam. This process also has the added benefit of not heating up the crystal. [2]

2.2 Simulation

A simulation was performed to show the effects of the OPCPA, more specifically the OPA, on the spatial properties of the different wavelengths in the beam. The Appendix section A.1 shows the Matlab codes. ooe phase matching was used, which means that the polarizations of the signal and idler are ordinary and pump is extraordinary. In the Matlab code, firstly, the wavelengths of the signal beam λ are set up from $0.545\,\mu\mathrm{m}$ to $10\,\mu\mathrm{m}$. The wavelength of the pump is $\lambda_p = 0.515\,\mu\mathrm{m}$. The phase matching angle θ, which is the angle between the signal beam and the optical axis, is set-up from 20° to 25.7°, and the noncollinear angle, which is the angle between the signal beam and the pump beam, is set as $\alpha = 0^\circ$. Then, λ and θ are extended into equal size matrices λ_0 and θ_0. The matrix of the idler wavelength is calculated by

$$\lambda_i = \frac{1}{\frac{1}{\lambda_p - 1} - \frac{1}{\lambda_0 - 1}}$$

which is energy conservation and is shown in Figure 1 a). The indices of refraction for the signal, idler, and pump beams in the Beta-barium borate (BBO) crystal are recorded as n_{o1},

n_{o2}, and n_{e3} respectively. The phase mismatching is calculated with

$$\Delta k = \sqrt{\left(\frac{n_{e3}^2}{\lambda_p^2} + \frac{n_{o1}^2}{\lambda_0^2} - \cos(\alpha) \cdot \frac{n_{e3}}{\lambda_p} \cdot \frac{n_{o1}}{\lambda_0}\right)} - \frac{n_{o2}}{\lambda_i}$$

which is momentum conservation and is shown in Figure 1 b).

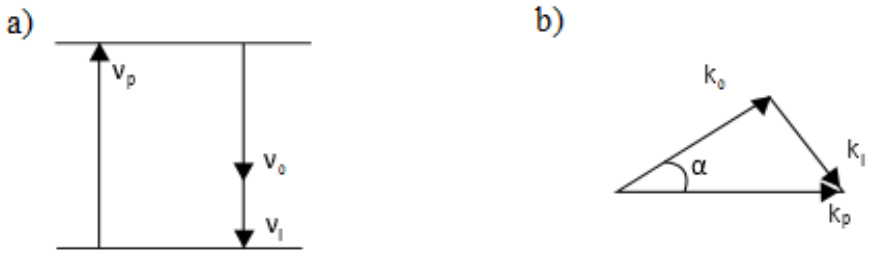

Figure 1: *The left diagram shows the energy conservation, and the right image shows the momentum conservation.*

Finally, the frequency ν is plotted against θ as shown in Figure 2. The same procedure was done for different values for $\alpha = 2.5°$. Both are shown in Figure 2. For the $\alpha = 2.5°$ image, at around $\theta = 24.4°$ in the frequency region of 300 THz to 425 THz, there is a band of wavelengths. This is the region where the OPCPA will work, creating a broadband situation.

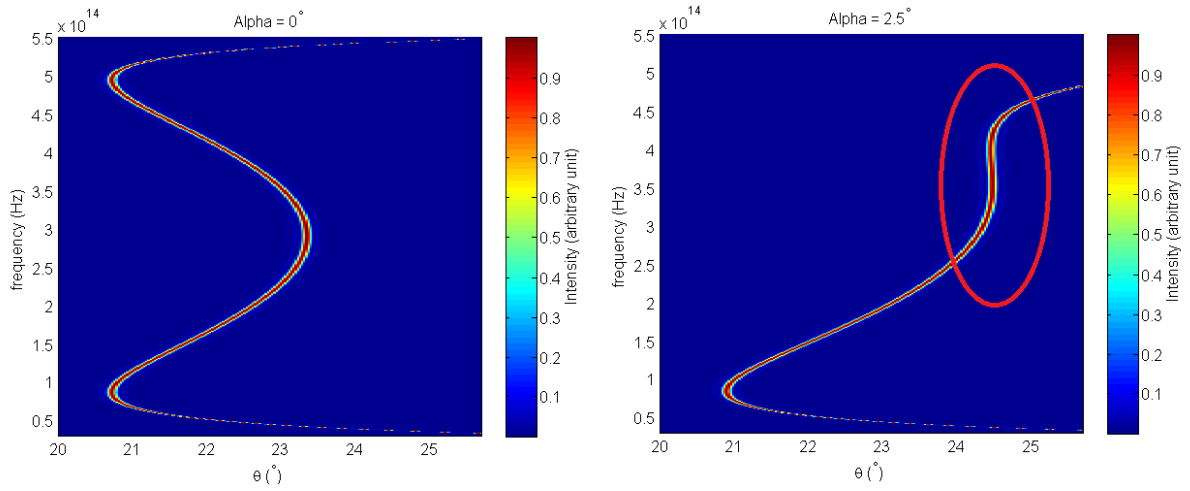

Figure 2: *The intensity of the beam for the phase matching angle of the pump θ for two different values for the noncollinear angle α. For $\alpha = 2.5°$, there is a band of wavelengths at around $\theta = 24.4°$ in the frequency region of* 300 THz *to* 425 THz*, shown by the red circle.*

The same information is presented in Figure 3, but in a more demonstrative way. Focusing the pump into the crystal makes the phase matching visible. One will see a ring of phase-matched wavelengths around the pump beam.

Figure 3 shows the frequencies versus different α values for a single value for θ. This is found by modifying the Matlab code. In the zoomed in image one can see that, going from high

frequencies (low wavelengths) to low frequencies (high wavelengths), the angle increases and then decreases slightly before increasing again. The image is symmetrical, so there will be a symmetrical increase in the radius of the beam profile for these wavelengths.

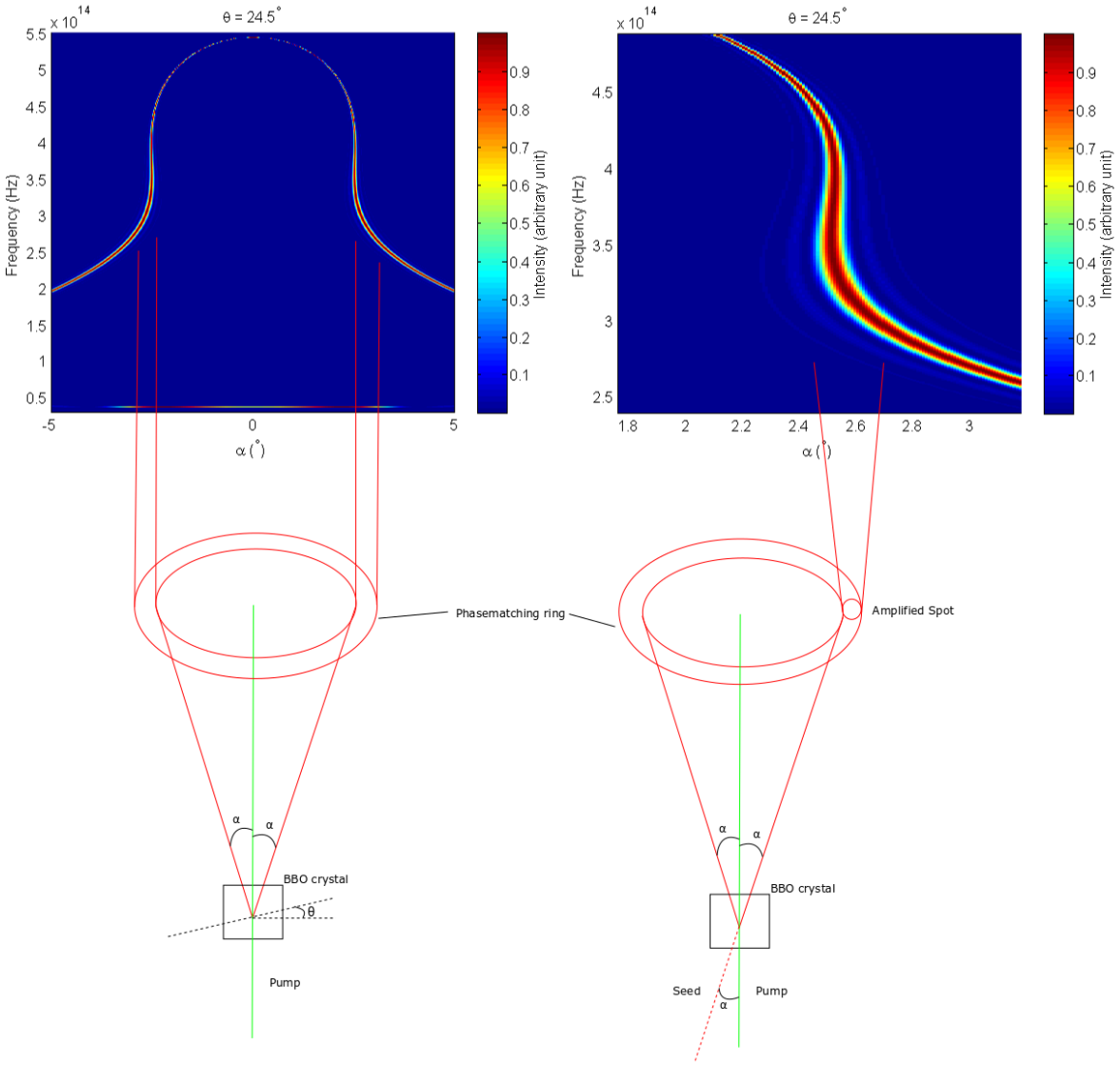

Figure 3: *The intensity of the beam for the frequencies for the noncollinear angle α for the value for the phase matching angle $\theta = 24.5°$, and a zoomed in image of the band of frequencies at $\alpha = 2.5$. The bottom part of the image shows the beam profile of the beam after the BBO crystal.*

3 Imaging Spectrometer

This section presents the set-up for the imaging spectrometer. It also shows the calibration of the spectrometer, and a comparison of different screens.

A spectrometer is a tool to measure the wavelengths from a light source. Most often, the intensity of the light is the variable measured. An imaging spectrometer differs from a normal spectrometer in the sense that it can also see the spatial component in one direction of the beam. In other words, it can observe angular dispersion or the width and position in space of each wavelength in the beam profile in that direction. There are two ways to use the spectrometer: the beam can be focused on the slit or it can be collimated. The spectrometer for the experiments used the latter way.

3.1 Set-up

Figure 4 shows the set-up for the spectrometer that was built for the experiments. Two mirrors were used to align the beam into the spectrometer (not shown). The slit diffracts the incoming laser light in the horizontal direction. The first mirror ($f = 30\,\mathrm{cm}$, $D = 2.5\,\mathrm{cm}$) then collimates the beam in this direction. The diffraction grating (600 groves per mm, 750 blaze wavelength, blaze angle of $13°$) diffracts the each wavelength at different angles. The next mirror ($f = 15\,\mathrm{cm}$, $D = 7.5\,\mathrm{cm}$) focuses in the horizontal direction the individual wavelengths on the screen, which is then viewed with the camera. The mirrors were spherical. The slit is adjustable up to 6 mm, which also means that the aperture is $6\,\mathrm{mm}$ high.

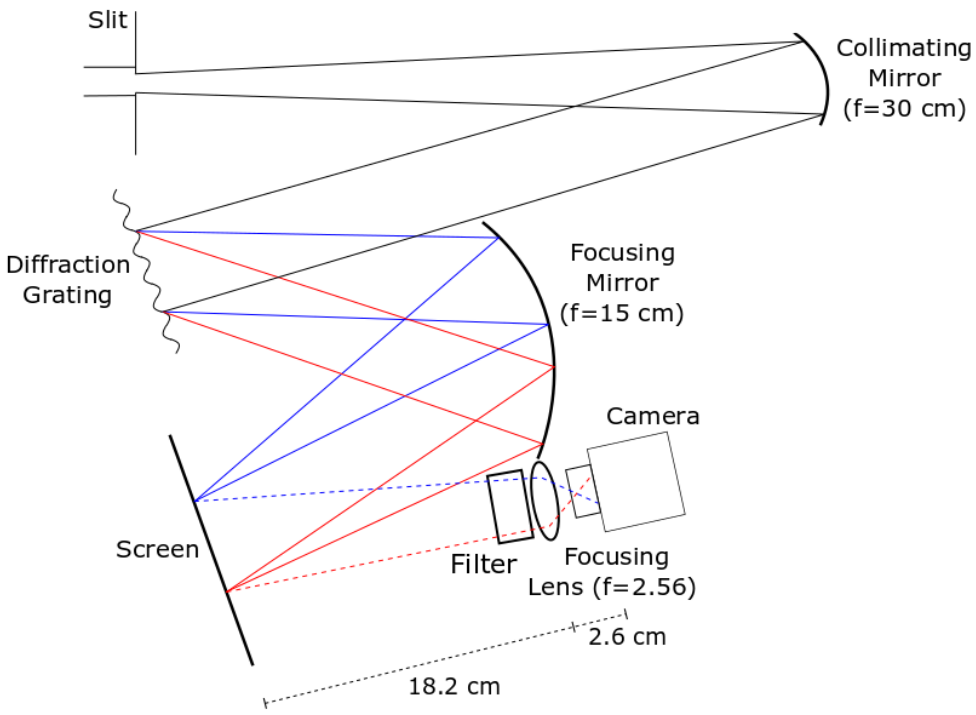

Figure 4: *A top-down view of the set-up for the spectrometer. The blue lines represent the low wavelengths and the red lines represent the high wavelengths. An adjustable pin-hole is placed in front of the slit and another between the slit and the collimating mirror. These are used to align the beam.*

Figure 5 shows the beam radius properties in the imaging spectrometer from a side-view perspective. The beam radius defined as the point of the beam from the beam axis where the intensity falls to $1/e^2$ [2]. The incoming beam is collimated. The diffraction grating is placed $30\,\mathrm{cm}$ from the collimating mirror in order to focus the beam on it. The focusing mirror with a focal length of $15\,\mathrm{cm}$ is placed $15\,\mathrm{cm}$ from the grating. Thus, the outgoing beam is approximately half the size of the incoming beam, and it is collimated enough, at least for the distance to the screen.

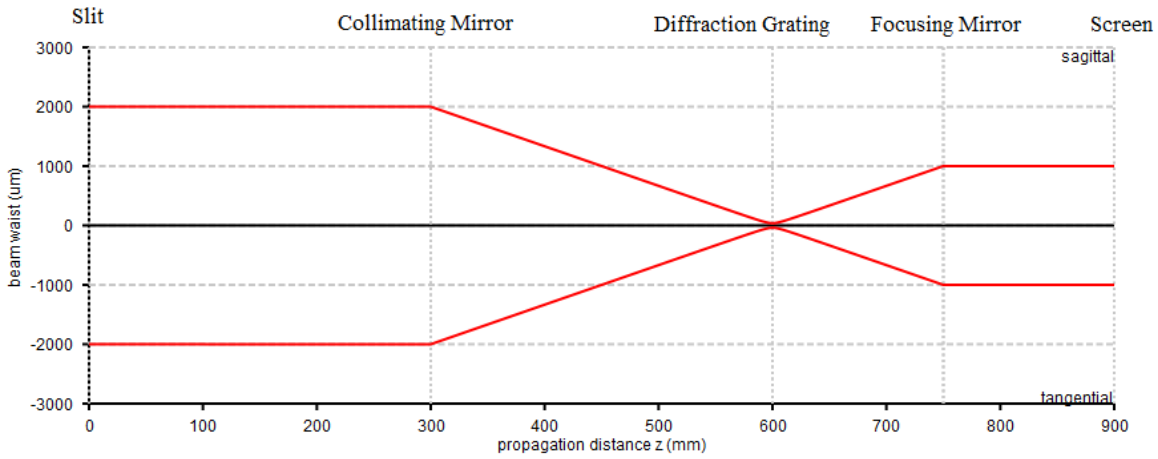

Figure 5: *The beam radius of the vertical component as calculated by the vWaistWatcher program. The incoming beam and the outgoing beam are both collimated, with the outgoing beam being approximately half the size. The slit size is 6 mm, and the incoming beam is approximately 4 mm.*

The camera chip has a size of $5.952\,\mathrm{mm}$ by $4.762\,\mathrm{mm}$. In pixels, the size of the image is 1280 by 1024. Thus, a millimeter is about 215 pixels. Larger chips of this kind are rare and expensive. A lens of focal length $f = 2.56\,\mathrm{cm}$ is placed in front of the camera in order to focus the image from the screen. The camera is placed $20.8\,\mathrm{cm}$ from the screen. The lens is placed $2.6\,\mathrm{cm}$ in front of the camera. Thus, the magnification is then about $\frac{2.6}{18.2} = \frac{1}{7}$ times. Also, reflective neutral density filters were placed in front of the camera to prevent saturation of the image and to prevent damage to the camera chip.

All the optical components are not evenly transmissive or reflective for all wavelengths, especially for broad bands of wavelengths like the $600\,\mathrm{nm}$ to $1100\,\mathrm{nm}$ from the Ti:Sapphire laser oscillator. These details are shown in Figure 6 below. For the mirrors, the reflectance is a few percent less at around 800 to $900\,\mathrm{nm}$ than at $600\,\mathrm{nm}$ and $1100\,\mathrm{nm}$. The diffraction grating has less efficiency for the higher wavelengths. The neutral density filters have the given transmission percentage at around 600 to $700\,\mathrm{nm}$. This percentage rises for the higher wavelengths.

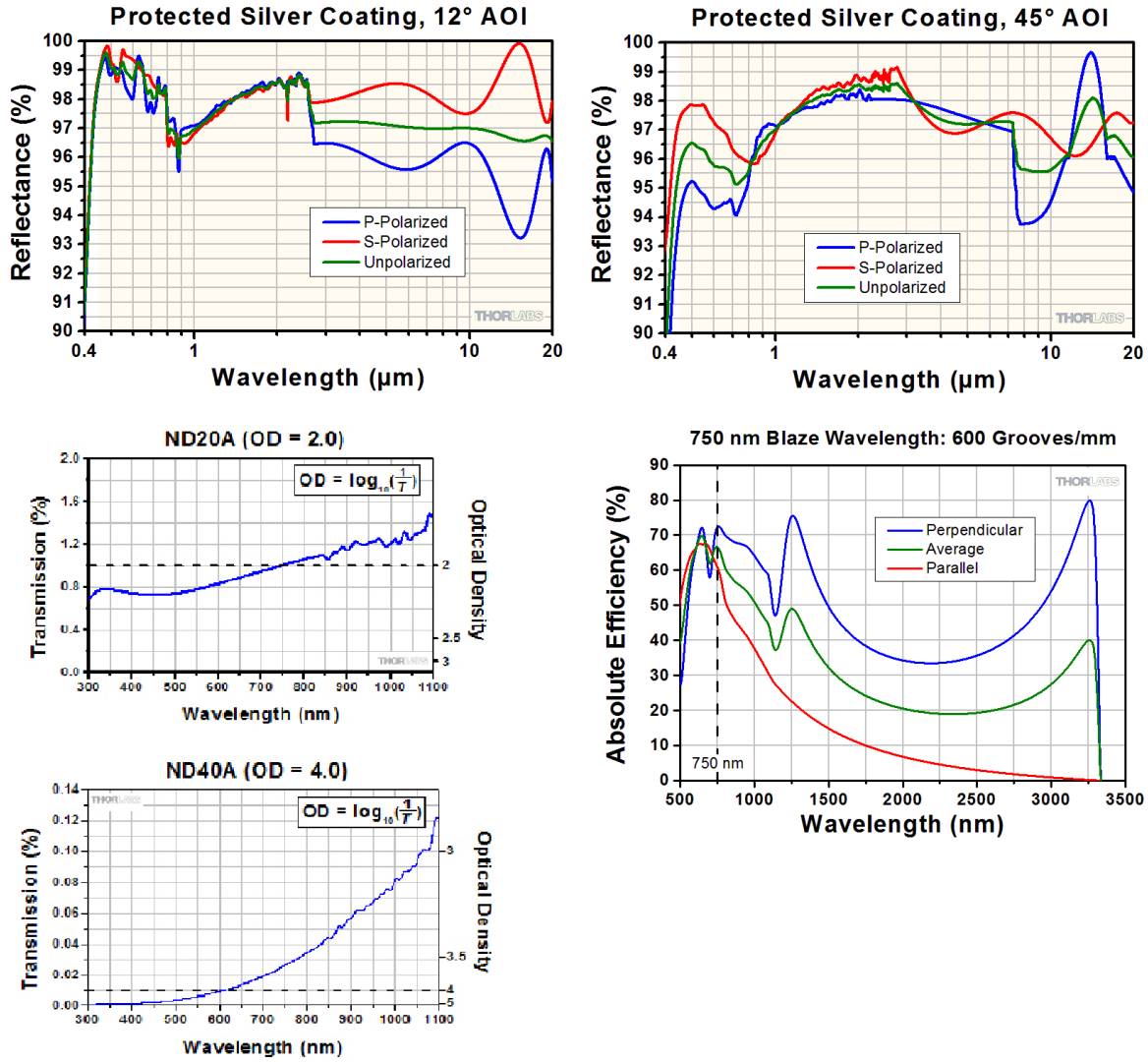

Figure 6: *Details for the Thorlabs equipment used taken from their website [3]. The region of interest is the band of wavelengths from 600 nm to 1100 nm. The two top graphs show the reflectance of the silver coated mirrors at two angles of incidence. The two graphs at the bottom left show the transmission of the two kinds of neutral density filters. The bottom right shows the efficiency of the diffraction grating.*

3.2 Wavelength and CCD Calibration

For the calibration of the spectrometer, four different spectral lamps with known wavelengths were used [4]. Neon and Cadmium have wavelengths close to 640 nm, and Rubidium and Argon have wavelengths close to 800 nm. The image of the spectra can be seen in Figure 7, and the values in Table 1 below. The calibration curve can be seen in Figure 8. The light from the lamps were focused on the slit in order to increase the intensity.

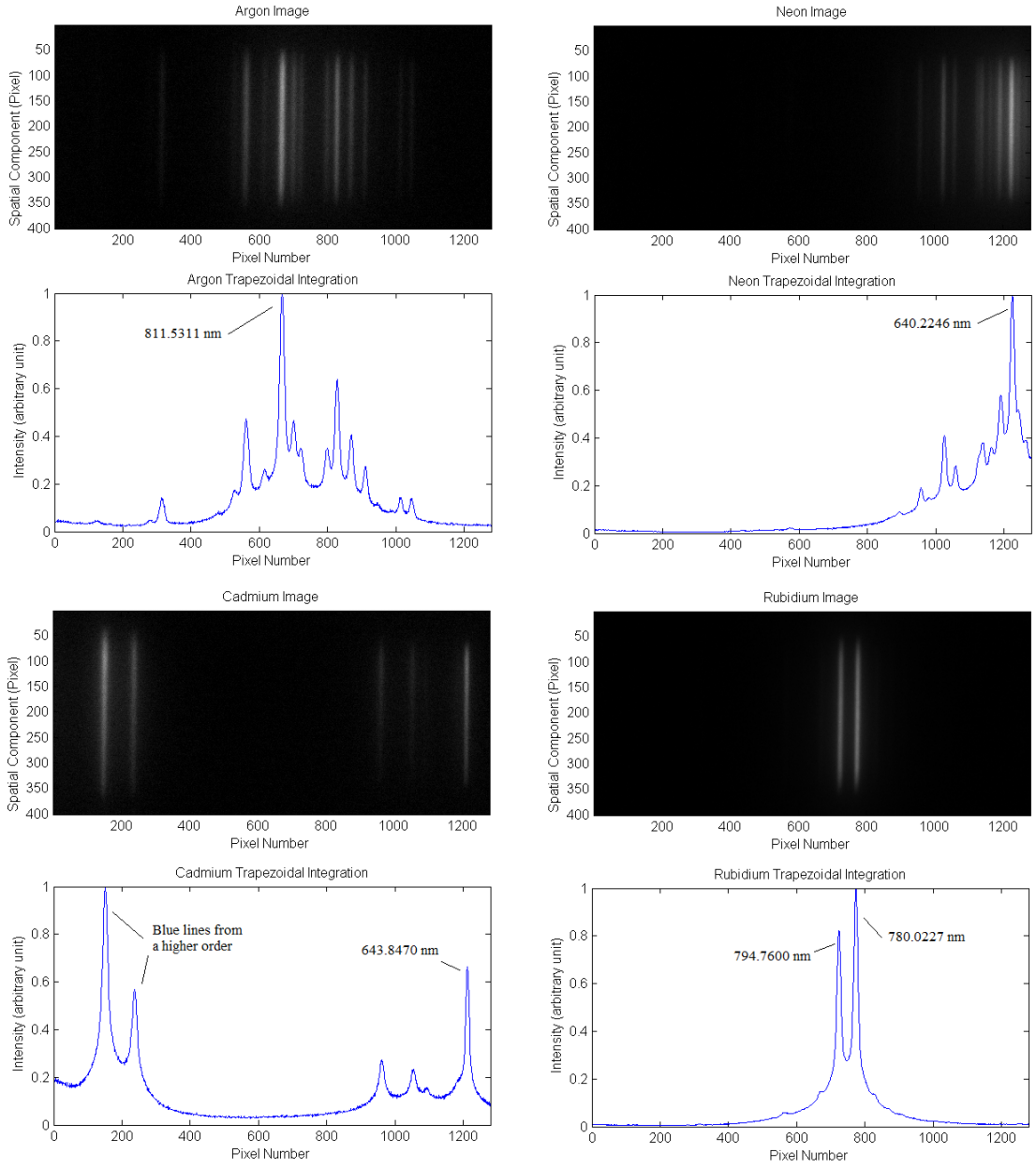

Figure 7: *The spectra from the four calibration lamps and the integrated spectra. The Argon line is actually two lines that are too close together to differentiate them. The high wavelength bright lines in the Cadmium spectrum are actually blue lines from a higher order. The integration allows the prominent wavelengths to be found more easily.*

In the CCD pictures of Figure 7, one can see that the lines are longer towards the left of the image, than to the right. This can be seen most clearly in the Cadmium spectrum. This may be due to a small difference in path length for the different wavelengths. If the screen was adjusted to make the heights the same, the wavelengths to one side of the screen would be out of focus.

In order to more easily find the position of each prominent line, each position on the x-axis was integrated across the y-axis. This is done using trapezoidal integration, which has

the form $I = \frac{1}{2}f(1) + f(2) + f(3) + ... + f(n-1) + \frac{1}{2}f(n)$. The Matlab function can be found in the Appendix section A.4. Figure 7 shows the integrated spectra for the four calibration lamps.

The Argon line is actually two lines, $810.3693\,\mathrm{nm}$ and $811.5311\,\mathrm{nm}$. The latter has higher intensity, so that line was used for the calibration.

Table 1: *The prominent wavelengths of the calibration lamps [4] and their respective pixel numbers from the camera.*

Lamp	λ from Ref. [4] (nm)	Pixel Number
Neon	640.2246	1225
Cadmium	643.8470	1212
Rubidium	780.0227	774
	794.7600	724
Argon	811.5311	667

Figure 8 shows the calibration curve for the spectrometer. The linear approximation of $y = -0.3085x + 1018$ is the best-fit line for the data points.

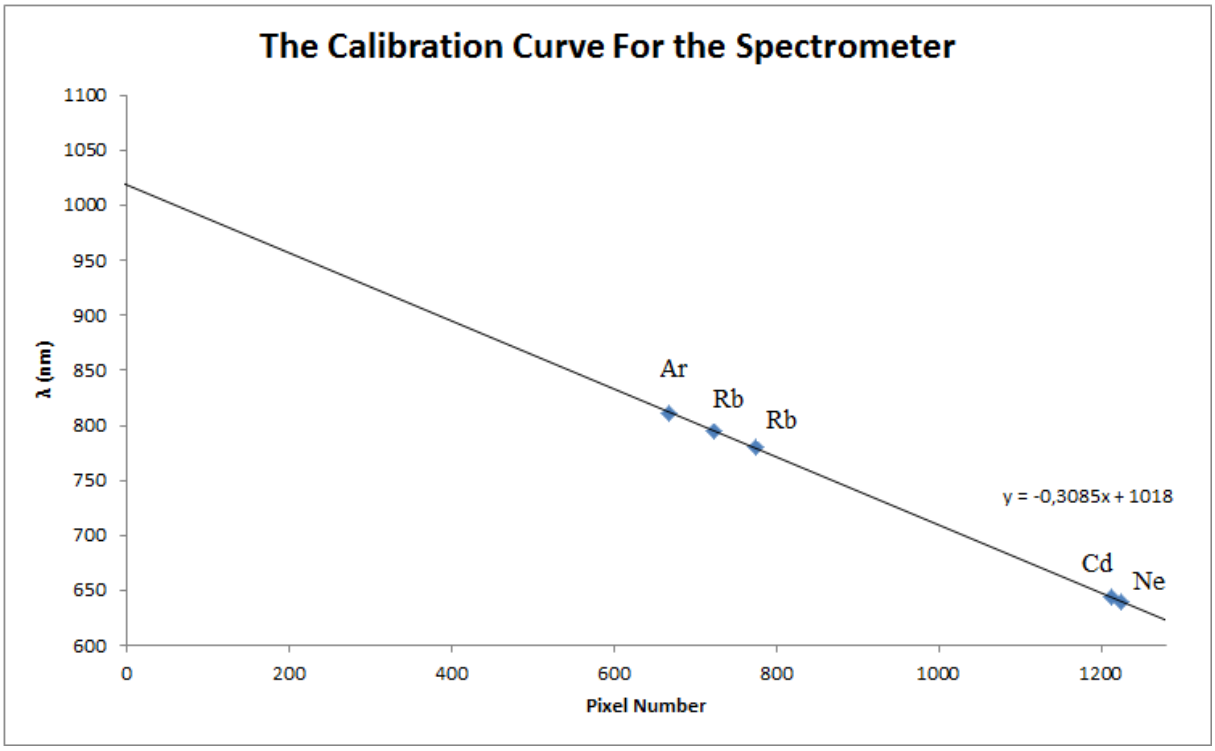

Figure 8: *The best-fit line for the data points from the calibration lamps with x being the pixel number of the camera and y being the corresponding wavelength.*

In order to test the accuracy of the calibration curve, the peaks of the Argon spectrum were measured with the calibration curve found in Figure 8. The measurements can be seen in Figure 9 and in Table 2. The difference becomes greater for the higher wavelengths. The calibration curve was deemed acceptable, and was used for subsequent calculations. This calibration will

also make the images appear inverted in the horizontal direction as opposed to due to the negative calibration curve.

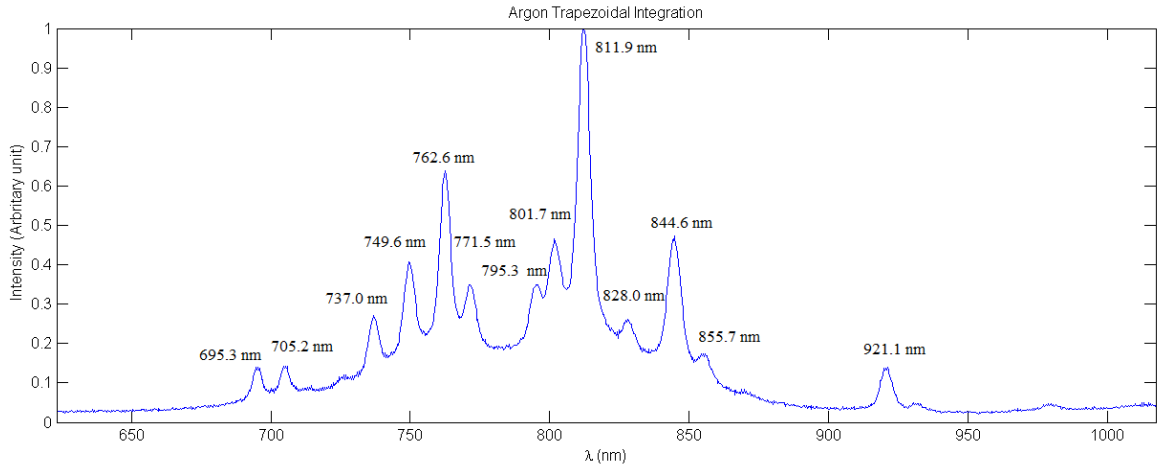

Figure 9: *The lines of the Argon spectrum with the peaks found using the calibration curve from Figure 8.*

Table 2: *A comparison between the measured peaks of the Argon spectrum versus the tabulated wavelengths [4]. If there are more than one line within a nm of each other, then the line with the highest intensity is used.*

Calibration λ (nm)	λ from Ref. [4] (nm)	$\Delta\lambda$ (nm)
695,3	696,5	1,2
705,2	706,7	1,5
737,0	738,4	1,4
749,6	750,4	0,8
762,6	763,5	0,9
771,5	772,4	0,9
795,3	794,8	-0,5
801,7	801,5	-0,2
811,9	811,5	-0,4
844,6	842,5	-2,1
855,7	852,1	-3,6
921,1	912,3	-8,8

3.3 Screen

Due to the broadband spectrum of the OPCPA laser (600 nm to 1100 nm) a special screen was needed. The camera chip was too small to focus the beam directly on it. Both white and black paper were tested using the beam from the oscillator only without the OPCPA, and the results are shown below in Figure 10. The white screen had a filter of optical density 4.0 (0.01%) and the camera was set to a gain of 7.87x. The black screen had a filter of optical density 2.0 (1%) and the camera was set to a gain of 1.00x.

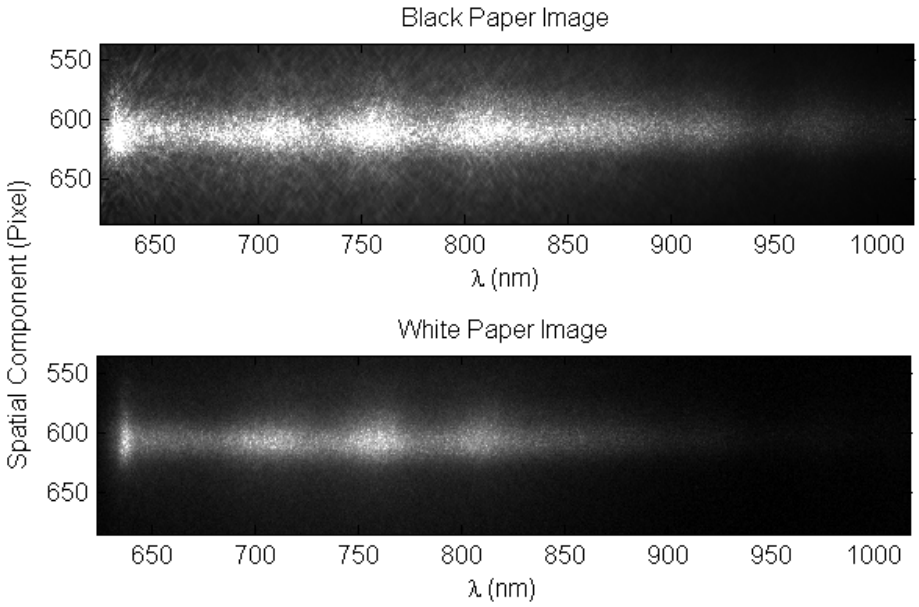

Figure 10: *A comparison of a white screen and a black screen. Black screen has higher intensity in the infrared region and seems to have a more even intensity overall. However, it also seems to have more noise and saturation in the signal.*

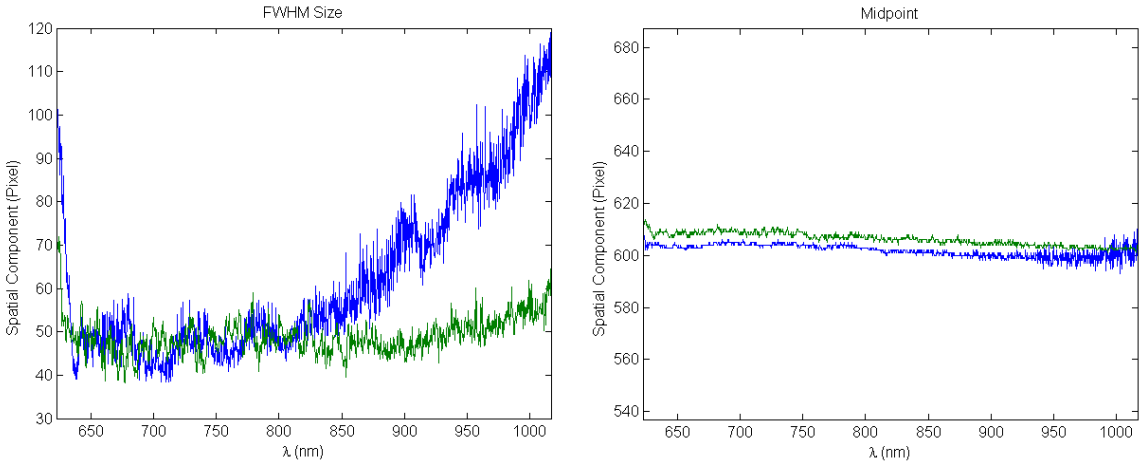

Figure 11: *The full-width half-maximum for each wavelength on the left and the midpoint on the right. The blue line represents the spectrum from the white paper, and the green line represents the spectrum from the black paper. The midpoint image is inverted in the y-direction with respect to the images in Figure 10.*

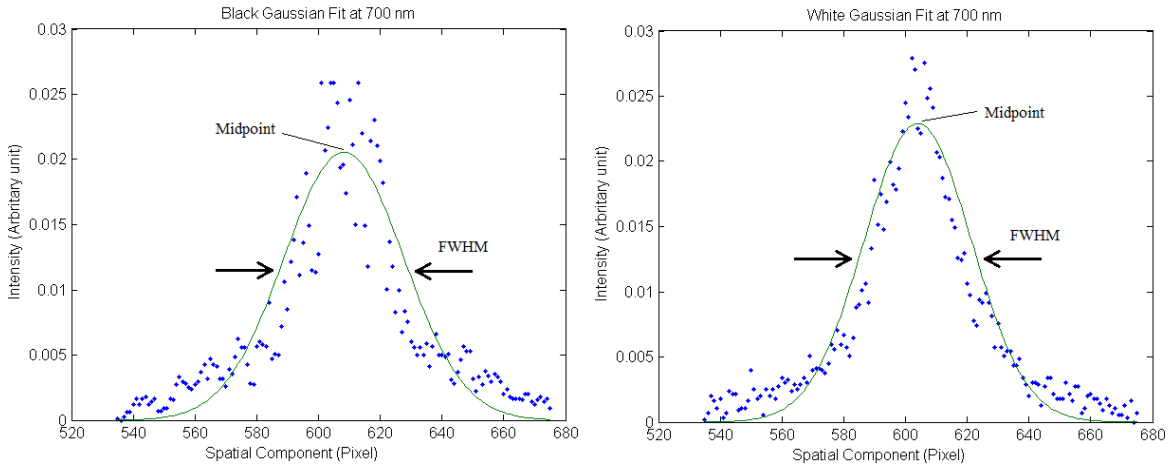

Figure 12: *The distribution at 700 nm for the black paper, left image, and the white paper, right image. The approximated Gaussian is also shown.*

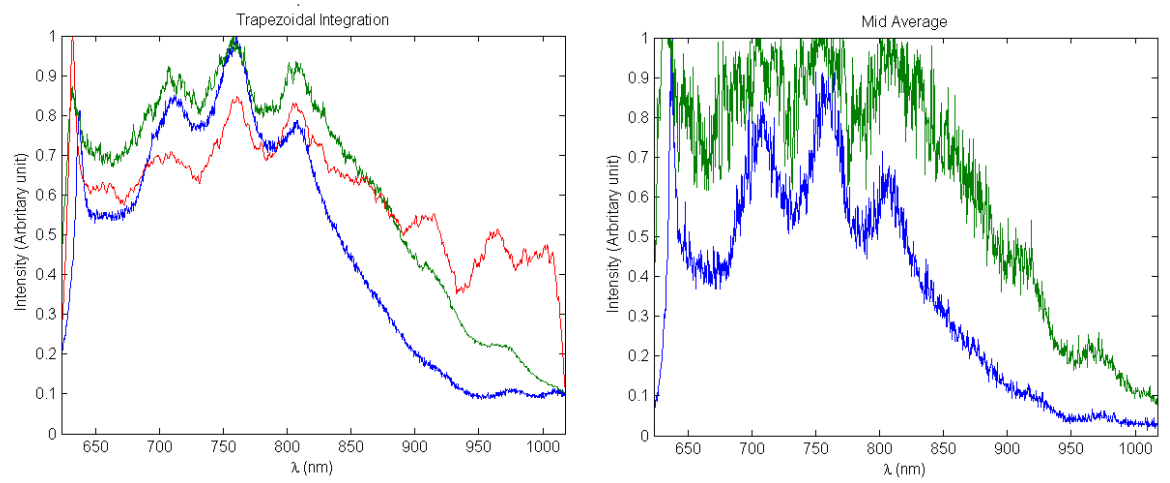

Figure 13: *The blue line represents the spectrum from the white paper, and the green line represents the spectrum from the black paper. The red line represents the data from the AQ6370C Optical Spectrum Analyser for comparison.*

The full-width half-maximum (FWHM) is found from first approximating the values to a Gaussian. Then, the width at half the maximum value was found. The Matlab code can be found in the Appendix section A.5. Looking at the FWHM size for each wavelength in Figure 11, the black paper has even values across the entire spectrum, while the white paper has increasing values due to less relative intensity for the higher wavelengths. Also, the Midpoint shows the midpoint of the Gaussian approximation. The image is slanted, but just by a few pixels, and one pixel represents about $32.6\,\mu\mathrm{m}$. This small offset is hard to adjust, and can come from any part of the spectrometer not being aligned perfectly. Figure 12 shows the cross-section of the spectrum at $700\,\mathrm{nm}$ with the approximated Gaussian. The noise and saturation can be seen in the image for the black paper. Both images have the problem that the maxima of the Gaussian do not match the maxima of the spectra. Also, tied in with this, the widths of the Gaussian seem to be slightly larger. The midpoint Figure 12 shows the Gaussian approximation

at $700\,\mathrm{nm}$ for both the black paper and the white paper. The Mid Average image in Figure 13 is in principle the same as the trapezoidal integration, except that only five points around the middle of the spectrum are added. The Matlab code can be found in the Appendix section A.3. The output value helps give a view of the noise in the signal. The black paper seems to have more noise than the white paper, which could be due to the black paper having a slightly rougher surface. However, the black paper has higher relative intensity for the higher wavelengths, which could be due to the fluorescence found in the white paper for visible light is not observed here.

Due to the higher relative intensities for the higher wavelengths, the black paper was chosen for the experiments. The purpose of the spectrometer is to find the spatial information of the beam. While there is a loss in intensity compared to the Optical Spectrum Analyser for the high wavelengths, as long as wavelengths are visible, the spatial information should be visible.

4 Experimental Results and Discussion

In order to test the spatial capabilities of the spectrometer, a prism wedge was placed in the beam path, which introduced a known amount of angular dispersion. Then, the output from the OPCPA was measured. Finally, the OPCPA beam was rotated 90 degrees to observe the beam profile in the other axis.

4.1 Prism Wedge

The angle of separation between the planes of the prism wedge was 4°. The material of the glass was N-BK7. The short wavelengths diverge less than the long wavelengths, which introduces an angle on the image on the screen. The wedge was placed 8 cm in front of the slit, and the beam was aligned to the spectrometer. The beam was not collimated afterwards, by using another prisma for example, as the divergence is small.

Figure 14 shows two spectra, the No Wedge Image is the same as the Black Paper Image from Figure 10, and the Wedge Image was taken with the prism wedge placed in the beam. The figure also shows the positions of the maxima of the approximated Gaussian distributions of the images. However, due to how Matlab handles vectors, the slope for the positions of the maxima is inverted with respect to the image.

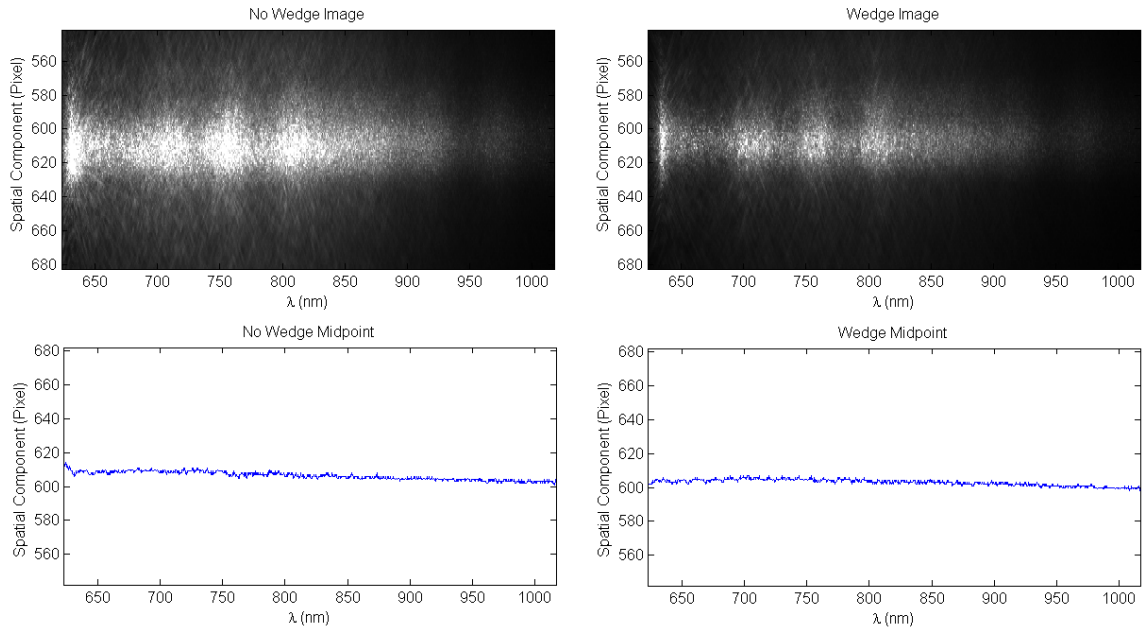

Figure 14: *The images obtained with a wedge and without a wedge, along with the position of the maxima of the approximated Gaussians. The wedge image has less intensity due to the reflections in the wedge. The angle of the slope of the positions of the maxima is inverted with respect to the images.*

In order to test the results, the following calculation was done. Two wavelengths were chosen for comparison, $700\,\mathrm{nm}$ and $900\,\mathrm{nm}$. For No Wedge Image, the positions of the maximum for $700\,\mathrm{nm}$ was 610, and the positions of the maximum for $900\,\mathrm{nm}$ was 604, which gives a difference of 6 pixels. For the Wedge Image, they are 606 and 602 respectively, which gives

a difference of 4 pixels. Thus, the wedge offsets the image by 2 pixels over this range. For the camera chip, there are 215 pixels per mm, and the image from the screen has magnification of $\frac{1}{7}$ on the chip, so a pixel on the camera chip represents $32.6\,\mu\text{m}$ on the screen. Therefore, the offset on the screen becomes:

$$2\,\text{pixels} \cdot \frac{1\,\text{mm}}{215\,\text{pixels}} \cdot 7 = 65.1\,\mu\text{m}$$

For small angles, the outgoing angle δ from a prism is

$$\delta \approx A(n-1)$$

where A is the angle between the two planes and n is the refractive index [5]. For the prism wedge, $A = 4° = 69.8\,\text{mrad}$. The refractive index for light of $700\,\text{nm}$ in N-BK7 glass is $n_{700nm} = 1.51306$ and for $900\,\text{nm}$ $n_{900nm} = 1.509$ [6]. The outgoing angles then become:

$$\delta_{700nm} = 0.0698 \cdot (1.52306 - 1) = 36.5\,\text{mrad}$$

$$\delta_{900nm} = 0.0698 \cdot (1.509 - 1) = 35.5\,\text{mrad}$$

The difference between these two angles is

$$\Delta\delta = \delta_{700nm} - \delta_{900nm} = 1.0\,\text{mrad}$$

Figure 15 shows the beam radius of a collimated beam and a $1.0\,\text{mrad}$ divergent beam. The individual wavelengths of $700\,\text{nm}$ and $900\,\text{nm}$ are collimated. Therefore, there is one collimated beam, for example $900\,\text{nm}$, aligned with the upper line of the divergent beam and one collimated beam, for example $700\,\text{nm}$, aligned with the lower line. Figure 15 shows the divergent beam and a collimated beam.

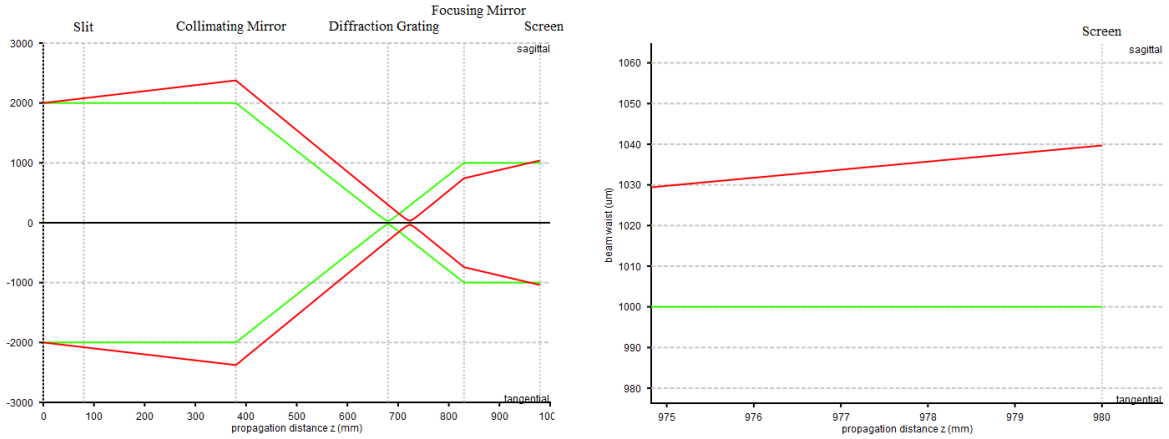

Figure 15: *The beam radius for the vertical component as calculated by the vWaistWatcher program. The right image is a magnification of the left at the screen. The green line shows a collimated beam, and the red line shows a beam with a divergence of* $1.0\,\text{mrad}$*. The green line has a beam radius of* $1000.01\,\mu\text{m}$*, and the red line has a beam radius of* $1039.67\,\mu\text{m}$*.*

The two wavelengths, $700\,\text{nm}$ and $900\,\text{nm}$, as shown in Figure 15, respectively have beam radi of $1000.01\,\mu\text{m}$ and $1039.67\,\mu\text{m}$, and thus, they have a separation of $79.32\,\mu\text{m}$. This is within the pixel size of $65.1\,\mu\text{m}$ on the image.

The prism wedge experiment shows that the set-up can measure the vertical component of the beam. The difference between the $700\,\mathrm{nm}$ and $900\,\mathrm{nm}$ positions of the two beams shown in Figure 14 is just two pixels. While, this does correspond with the theoretical calculations, the precision of the results can be improved. A prism with a greater angle between the two planes would diverge the wavelengths more, leading to a greater difference on the image. However, too much divergence could lead to varying the beam path length, which could lead to the image on the screen seeming to have greater divergence as seen with the increasing length for the high wavelengths seen in the calibration spectra in Figure 7. This can be reduced by collimating the beam using a second prism.

4.2 OPCPA

The amplified beam from the OPCPA was directed into the spectrometer. Slightly different positions of alignment were tested by adjusting the angles of the two alignment mirrors to look at different parts of the beam.

Figure 16 shows four slightly different alignment positions for the amplified beam. For position 1 the camera had a gain of 7.97x, for position 2 the camera had a gain of 8.98x, and for positions 3 and 4 the camera had a gain of 13.66x. Positions 1 and 2 show two different vertical positions. There are no noticeable differences between the two, except for the vertical position. For the integrated spectra, positions 1 and 2 are almost the same. This is expected as the spectrometer should not affect the vertical component. Positions 2, 3, and 4 show three different horizontal positions. Positions 2, 3, and 4 have different intensity spectra. However, the peaks are in similar positions. No FWHM measurements were made due to the non-Gaussian properties of the beam and that the maximum is not always in the center of the spectra.

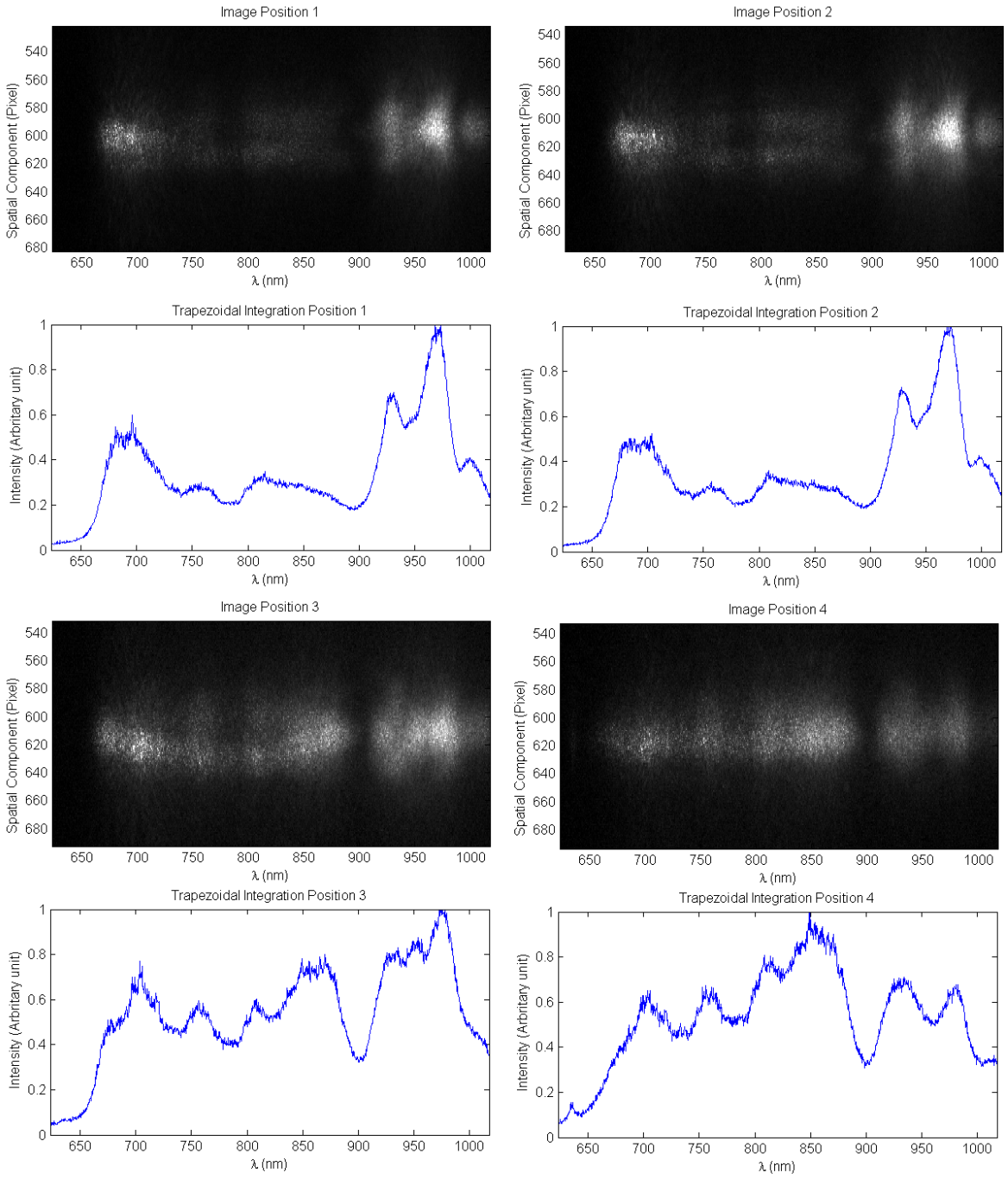

Figure 16: *Four positions along the beam along with their integrated spectra. Position 1 and 2 are the same horizontal position, but a different vertical position. Positions 2, 3, and 4 are taken at the same vertical position, but with different horizontal positions. For position 1 the camera had a gain of 7.97x, for position 2 the camera had a gain of 8.98x, and for positions 3 and 4 the camera had a gain of 13.66x.*

Looking at positions 2 and 3, the beam diverges in the region $700\,\mathrm{nm}$ to $850\,\mathrm{nm}$, leaving a small gap in the middle. Position 4 seems to be coupled the best, due to the power distribution. It is clear that the spectra are different from each other.

Due to the absorption and reflection of different wavelengths in the optical equipments and the surface of the screen, precise and accurate measurements are difficult to make. Using the screen can be avoided if the image can focused on the camera directly instead. The wide range of wavelengths makes this difficult. Bigger cameras of the type used are rare and expensive. The individual wavelengths, the horizontal component of the beam, and the vertical component of the beam all have different beam radii. Inserting more mirrors to further focus the beam makes aligning all three aspects of the beam more complex. Using a set-up that allows the camera to be moved along the beam at the focal point of the individual wavelengths allows the beam to be wider. Complications arise in the calibration of this system. Using lenses instead of mirrors can possibly decrease the difference in the path length of the beams, but at the cost of a longer, less compact set-up and possible chromatic and spherical aberrations.

4.3 Rotated Beam

The beam of the OPCPA is not uniform in all directions. Therefore, a periscope was used to rotate the amplified beam by 90°. This is done by placing a mirror to direct the beam upwards, and then placing another mirror to direct the beam perpendicular to the incoming beam.

Figure 17, shows the images for the beam rotated 90 degrees. Four different amplification positions were recorded; no amplifier and amplified at low, middle, and high wavelengths. The types of measurements were different for these images than before due to the amplification being much weaker for these.

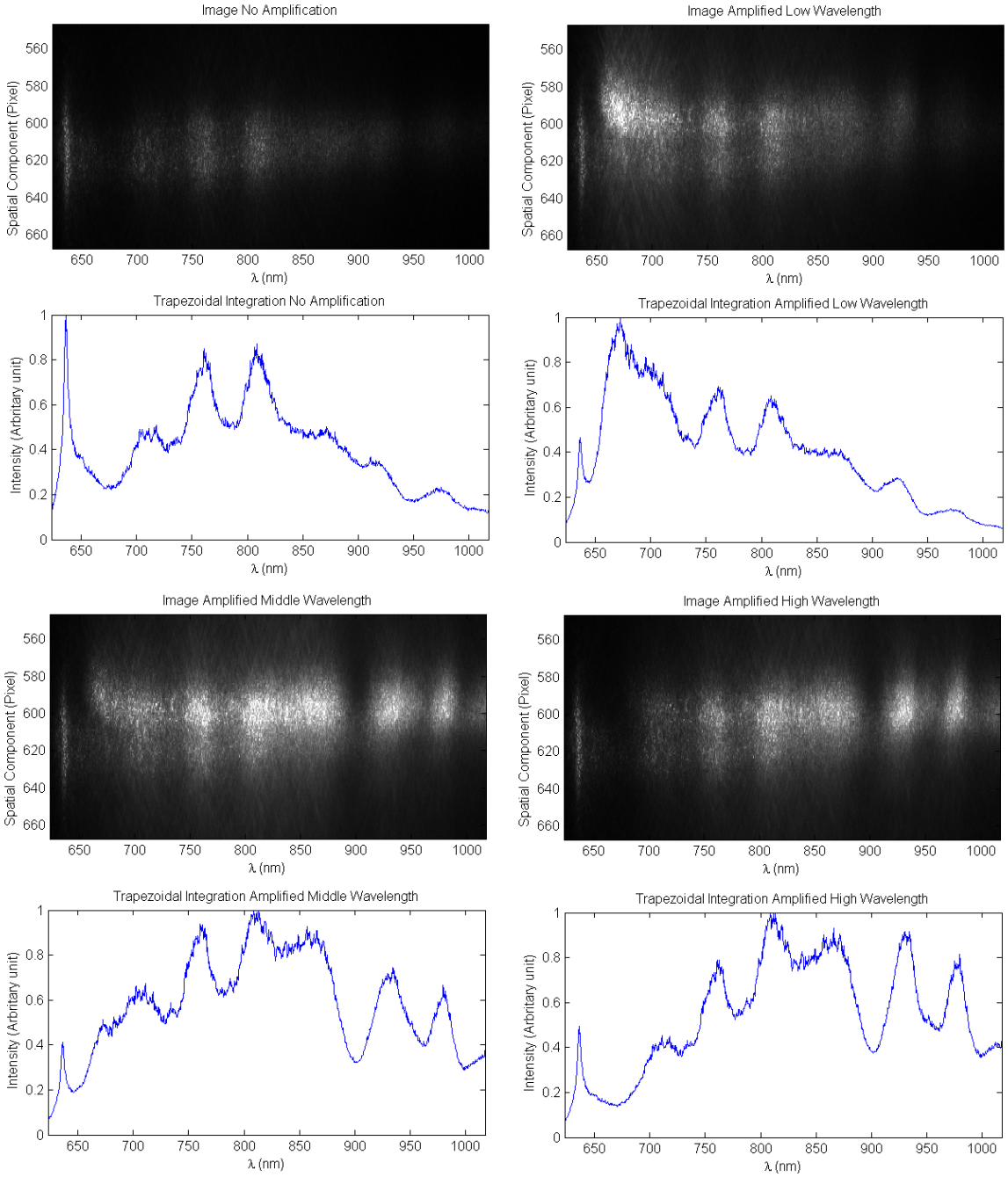

Figure 17: *The images for the rotated beam with amplification at different positions. The camera has the same gain of 2.02x for all images.*

The rotated beam experiment shows that the beam is not uniform in all directions. The seed can be seen below the OPCPA spectra, which interfers with potential measurements. Subtracting the no amplification image from the other images could lead to possible analysis. It also shows that the intensity can greatly vary due to the alignment in the OPCPA.

5 Conclusions and Outlook

The purpose of the thesis was to build a imaging spectrometer to observe the spatial properties of the beam profile of the OPCPA output. In the Theory section, the origin of the angular dispersion was presented and discussed. It is most prominent for the most broadband phase-matched situation. An imaging spectrometer was designed, built, and calibrated with spectral lamps and tested. The wedge experiment showed that it could measure the spatial distance. The OPCPA showed that the beam profile is different for slightly different adjustments in the alignment of the beam. The need to use of a screen, and also the absorption and reflection in the different optical equipments, made accurate and precise measurements difficult. The rotated OPCPA beam experiment showed a different result than intended. It shows difficulties that need to be improved in further investigation. Altogether, the imaging spectrometer served the purpose for which it was made as it could observe the beam profile of the OPCPA beam.

The main cause for the difficulty in the set-up and the experiments was the broad band of wavelengths, $600\,\mathrm{nm}$ to $1100\,\mathrm{nm}$, in the beam. The focusing mirror needed to be $7.5\,\mathrm{cm}$ in diameter and placed $15\,\mathrm{cm}$ from the grating in order for the entire beam from the grating to fit on the mirror. This is also most likely the origin for the different path lengths leading to the increasing length in the vertical component seen in Figure 7. The spectra are smaller in this direction, so the effect is small. The broad band also led to the need for using a screen instead of just focusing the beam on the camera. Some spatial information and intensity is lost on the screen. These problems could be minimized by either using a diffraction grating with less grooves per mm or only looking at parts of the spectrum at a time.

Another interesting experiment would be to focus the beam from the OPCPA onto a sapphire crystal. If placed correctly, it should generate a ”cone” of wavelengths. This will show up on the image in a triangular shape as one side of the wavelengths will be wide and the other will be short.

Using cylindrical mirrors instead to spherical mirrors can eliminate the need to worry about the vertical direction of the beam through optical components of the spectrometer. They will, however, need a more careful alignment than their spherical counterparts.

Another set-up would be to focus the beam onto the slit instead of having it be collimated. This method, made easier with the cylindrical mirrors, can give a measurement of the non-collinear angle α instead of the spatial component, or at least relative measurements of the angle.

A Matlab Codes

A.1 Simulation

The simulation codes are based on the work done by Chen Guo, PhD student at Lund's University and expanded upon by Mattias Bengtsson.

A.1.1 Phase Matching Angle

```
clear all;
clc;
clf;
%ooe phase matching. The signal and idler are o and pump is e

wl=[0.545:0.001:10];%Wavelength of signal in micro
wlp=0.515;%Wavelength of pump
% angle=[1*pi/9:0.0001:1*pi/7]';%Phase matching angle of pump in rad
theta=[1*pi/9:.0005:1*pi/7]';%Phase matching angle of pump in rad
l=length(theta);
alpha=deg2rad(2.5);%Noncollinear angle
%alpha=degtorad(0);%Noncollinear angle
lw=length(wl);

wl0=wextend('ar','spd',wl,l-1,'r');%Matrix of wavelength
theta0=wextend('ac','spd',theta,lw-1,'r');%Matrix of phase matching angle
wli=1./(1/wlp - 1./wl0);%Matrix of idler wavelength ENergy conservation

no1=BBO(wl0,0);%Index of refraction of signal
no2=BBO(wli,0);%Index of refraction of idler
ne3=BBO(wlp,theta0);%Index of refraction of pump

dk=sqrt(ne3.^2/wlp^2 + no1.^2./wl0.^2 - 2*cos(alpha) .* ne3./wlp .* no1./wl0) - no2./wli
im=sinc(dk*3000).^2;%Intensity

s=sum(im,2);
id=s==max(s);%Finding the best phase matching angle

c = 3e8;

%%% FIGURES %%%

figure(1);
plot(c ./ (wl .* 1e-6),im(id,:),'g');
xlabel('frequency (hz)');
ylabel('Efficiency (a.u.)');


figure(2);
pcolor(radtodeg(theta)',c ./ (wl'*1e-6),im')
shading flat
set(gca,'YDir','normal');
colorbar
title('Alpha = 0^{\circ}')
```

```
xlabel('\theta (degree)');
ylabel('frequency (hz)');
```

A.1.2 Noncollinear Angle

```
clear all;
clc;
clf;
%ooe phase matching. The signal and idler are o and pump is e

%%% Inputs %%%
thetaC = 79; % Phase matching angle looked at, theta = (thetaC-1)*0.001 + pi/9
del_alpha = degtorad(0.01);
min_alpha = degtorad(-5.0);
max_alpha = degtorad(5.0);

%%% Variables and formulas and functions %%%

alpha = min_alpha:del_alpha:max_alpha; %Noncollinear angle
n = length(alpha);

wl=(0.545:0.001:10);%Wavelength of signal in micro
wlp=0.515;%Wavelength of pump
% angle=[1*pi/9:0.0001:1*pi/7]';%Phase matching angle of pump in rad
theta=(1*pi/9:.001:1*pi/7)';%Phase matching angle of pump in rad
l=length(theta);
lw=length(wl);

wl0=wextend('ar','spd',wl,l-1,'r');%Matrix of wavelength
theta0=wextend('ac','spd',theta,lw-1,'r');%Matrix of phase matching angle
wli=1./(1/wlp - 1./wl0);%Matrix of idler wavelength ENergy conservation

no1=BBO(wl0,0);%Index of refraction of signal
no2=BBO(wli,0);%Index of refraction of idler
ne3=BBO(wlp,theta0);%Index of refraction of pump

c = 3e8; %speed of light

im2 = zeros(n,lw);

for ii = 1:n
    dk=sqrt(ne3.^2/wlp^2 + no1.^2./wl0.^2 - 2*cos(alpha(ii)) .* ne3./wlp .* no1./wl0) -
    im=sinc(dk*3000).^2;%Intensity

    im2(ii,:) = im(thetaC,:);
end

figure(1);
pcolor(radtodeg(alpha'),c ./ (wl'*1e-6),im2')
shading flat
set(gca,'YDir','normal');
colorbar
title('Theta = 79^{\circ}')
xlabel('\alpha (degree)');
ylabel('Frequency (hz)');
```

A.1.3 Index of Refraction in the Beta-Barium Borate (BBO) Crystal

```
function nes=BBO(wl,angle)
%angle is in rad
no2=2.7359+0.01878./(wl.^2-0.01822)-0.01354*wl.^2;
ne2=2.3753+0.01224./(wl.^2-0.01667)-0.01416*wl.^2;
nes=1./sqrt(cos(angle).^2./no2+sin(angle).^2./ne2);
```

A.2 Calibrations

```
% This function takes the range of the image wanted and applies the
% calibration curves to the axes.

function [x_cal y_cal] = func_cal(x_min,x_max,y_min,y_max)

for ix = x_min:x_max
    x_cal(ix) = -0.3085 * ix + 1018; %y = -0,3085x + 1018
end
y_cal = y_min:y_max;
end
```

A.3 Mid Average

```
% func_mid takes the stated mid point line of the x-axis of the spectrum
% in addition to two lines above and two lines below and averages the
% values.

function mid_avg = func_mid(Im,y_mid)

A = uint16(Im);

for ix = 1:1280
    a = A(y_mid - 2,ix,1);
    b = A(y_mid - 1,ix,1);
    c = A(y_mid,ix,1);
    d = A(y_mid + 1,ix,1);
    e = A(y_mid + 2,ix,1);
    B(1,ix) = (a + b + c + d + e) / 5;
end

C = double(B);
mid_avg = C / max(C);
end
```

A.4 Trapezoidal Integration

```
% func_Trape takes a trapezoidal integration across the y-axis of the
% image. Trapezoidal integration from 1 to n has the formula I = 1/2 *
% f(1) + f(2) +  f(3) + ... + f(n-1) + 1/2 * f(n).  f(1) and f(n) can be
% assumed to have no effect for the images for the spectra, so they do not
```

```
% need the 1/2 coefficient.

function Trape = func_Trape(Im,x_min,x_max,y_min,y_max)

A = uint16(Im);

A2 = A(:,:,1);

Trape = zeros(x_min,x_max);

for ix = x_min:x_max
    for iy = y_min:y_max
        Trape(ix) = Trape(ix) + A2(iy,ix);
    end
end

Trape = Trape / max(Trape);

end
```

A.5 FWHM

A.5.1 Main Function

```
% func_FWHM take the Full-Width Half-Maximum across the spectrum.  mu0 and
% sigma0 are two estimate values to increase the efficiency of the gaussfit
% function.  The midpoint is also calculated using the maximum position of
% the Gaussian fit

function [Y_fwhm Midpoint] = func_FWHM(Im,x_min,x_max,y_min,y_max,y_range)

A = uint16(Im);
A2 = A(:,:,1);
A3 = double(A2);

mu0  = 603.8;
sigma0 = 27.89;
y = y_min:y_max;

for ix = x_min:x_max
    for iy = 1:y_range
        Y(1,iy) = A3(iy + min(y) + 1,ix);
    end

    Y = Y - min(Y);
    Y_norm = Y/sum(Y);

    [sigma,mu] = gaussfit(y,Y_norm,sigma0,mu0);
    xp = y_min:1:y_max;
    yp = 1/(sqrt(2*pi)* sigma ) * exp( - (xp-mu).^2 / (2*sigma^2));

    Y_fwhm(ix) = fwhm_func2(xp,yp);

    [yp_max, I] = max(yp);
    Midpoint(ix) = xp(I);
```

```
end
end
```

A.5.2 Fitting a Gaussian

This code is mainly the work of Przemyslaw Baranski uploaded to the MATLAB Central File Exchange [7].

```
function [sigma, mu] = gaussfit( x, y, sigma0, mu0 )
% [sigma, mu] = gaussfit( x, y, sigma0, mu0 )
% Fits a guassian probability density function into (x,y) points using iterative
% LMS method. Gaussian p.d.f is given by:
% y = 1/(sqrt(2*pi)*sigma)*exp( -(x - mu)^2 / (2*sigma^2))
% The results are much better than minimazing logarithmic residuals
%
% INPUT:
% sigma0 - initial value of sigma (optional)
% mu0 - initial value of mean (optional)
%
% OUTPUT:
% sigma - optimal value of standard deviation
% mu - optimal value of mean
%
% REMARKS:
% The function does not always converge in which case try to use initial
% values sigma0, mu0. Check also if the data is properly scaled, i.e. p.d.f
% should approx. sum up to 1
%
% VERSION: 23.02.2012
%
% EXAMPLE USAGE:
% x = -10:1:10;
% s = 2;
% m = 3;
% y = 1/(sqrt(2*pi)* s ) * exp( - (x-m).^2 / (2*s^2)) + 0.02*randn( 1, 21 );
% [sigma,mu] = gaussfit( x, y )
% xp = -10:0.1:10;
% yp = 1/(sqrt(2*pi)* sigma ) * exp( - (xp-mu).^2 / (2*sigma^2));
% plot( x, y, 'o', xp, yp, '-' );


% Maximum number of iterations
Nmax = 50;

if( length( x ) ~= length( y ))
    %fprintf( 'x and y should be of equal length\n\r' );
    %exit;
end

n = length( x );
x = reshape( x, n, 1 );
y = reshape( y, n, 1 );

%sort according to x
X = [x,y];
```

```
X = sortrows( X );
x = X(:,1);
y = X(:,2);

%Checking if the data is normalized
dx = diff( x );
dy = 0.5*(y(1:length(y)-1) + y(2:length(y)));
s = sum( dx .* dy );
if( s > 1.5 | s < 0.5 )
    %fprintf( 'Data is not normalized! The pdf sums to: %f. Normalizing...\n\r', s );
    y = y ./ s;
end

X = zeros( n, 3 );
X(:,1) = 1;
X(:,2) = x;
X(:,3) = (x.*x);


% try to estimate mean mu from the location of the maximum
[ymax,index]=max(y);
mu = x(index);

% estimate sigma
sigma = 1/(sqrt(2*pi)*ymax);

if( nargin == 3 )
    sigma = sigma0;
end

if( nargin == 4 )
    mu = mu0;
end

%xp = linspace( min(x), max(x) );

% iterations
for i=1:Nmax
%    yp = 1/(sqrt(2*pi)*sigma) * exp( -(xp - mu).^2 / (2*sigma^2));
%    plot( x, y, 'o', xp, yp, '-' );

    dfdsigma = -1/(sqrt(2*pi)*sigma^2)*exp(-((x-mu).^2) / (2*sigma^2));
    dfdsigma = dfdsigma + 1/(sqrt(2*pi)*sigma).*exp(-((x-mu).^2) / (2*sigma^2)).*((x-mu)

    dfdmu = 1/(sqrt(2*pi)*sigma)*exp(-((x-mu).^2)/(2*sigma^2)).*(x-mu)/(sigma^2);

    F = [ dfdsigma dfdmu ];
    a0 = [sigma;mu];
    f0 = 1/(sqrt(2*pi)*sigma).*exp( -(x-mu).^2 /(2*sigma^2));
    a = (F'*F)^(-1)*F'*(y-f0) + a0;
    sigma = a(1);
    mu = a(2);

    if( sigma < 0 )
        sigma = abs( sigma );
        fprintf( 'Instability detected! Rerun with initial values sigma0 and mu0! \n\r'
```

```
        fprintf( 'Check if your data is properly scaled! p.d.f should approx. sum up to
        %exit;
    end
end
```

A.5.3 FWHM

This code is mainly the work of Patrick Egan uploaded to the MATLAB Central File Exchange [8].

```
function width = fwhm_func2(x,y)

% function width = fwhm(x,y)
%
% Full-Width at Half-Maximum (FWHM) of the waveform y(x)
% and its polarity.
% The FWHM result in 'width' will be in units of 'x'
%
%
% Rev 1.2, April 2006 (Patrick Egan)


y = y / max(y);
N = length(y);
lev50 = 0.5;
if y(1) < lev50                  % find index of center (max or min) of pulse
    [garbage,centerindex]=max(y);
    Pol = +1;
else
    [garbage,centerindex]=min(y);
    Pol = -1;
end
i = 2;
while sign(y(i)-lev50) == sign(y(i-1)-lev50)
    i = i+1;
end                                    %first crossing is between v(i-1) & v(i)
interp = (lev50-y(i-1)) / (y(i)-y(i-1));
tlead = x(i-1) + interp*(x(i)-x(i-1));
i = centerindex+1;                     %start search for next crossing at center
while ((sign(y(i)-lev50) == sign(y(i-1)-lev50)) & (i <= N-1))
    i = i+1;
end
if i ~= N
    Ptype = 1;
    interp = (lev50-y(i-1)) / (y(i)-y(i-1));
    ttrail = x(i-1) + interp*(x(i)-x(i-1));
    width = ttrail - tlead;
else
    Ptype = 2;
    ttrail = NaN;
    width = NaN;
end
```

References

[1] Boyd, Robert W. Nonlinear Optics. 3rd ed. Burlington, MA: Academic, 2008. Print.

[2] Paschotta, Rüdiger, Dr. Encyclopedia of Laser Physics and Technology. RP Photonics Consulting GmbH, n.d. Web. 25 July 2014. <http://www.rp-photonics.com/encyclopedia.html>.

[3] Thorlabs, Inc. - Your Source for Fiber Optics, Laser Diodes, Optical Instrumentation and Polarization Measurement & Control. Thorlabs, Inc., 2014. Web. 11 July 2014. <http://www.thorlabs.de/>.

[4] Sansonetti, J. E., and W. C. Martin. "Handbook of Basic Atomic Spectroscopic Data." NIST Handbook of Basic Atomic Spectroscopic Data. National Institute of Standards and Technology, 13 Nov. 2013. Web. 25 July 2014. <http://www.nist.gov/pml/data/handbook/index.cfm>

[5] Pedrotti, Frank L., Leno S. Pedrotti, and Leno Matthew. Pedrotti. Introduction to Optics. 3rd ed. Upper Saddle River, NJ: Pearson Prentice Hall, 2007. Print.

[6] Polyanskiy, Mikail N. "Refractive Index Database." Refractive Index Database. N.p., 2013. Web. 27 July 2014. <http://refractiveindex.info/>.

[7] Baranski, Przemyslaw. "Gaussian Fit." MATLAB Central. The MathWorks, Inc., 23 Feb. 2012. Web. 11 July 2014. <http://www.mathworks.com/matlabcentral/fileexchange/35122-gaussian-fit>.

[8] Egan, Patrick. "fwhm." MATLAB Central. The MathWorks, Inc., 05 Apr. 2006. Web. 11 July 2014. <http://www.mathworks.com/matlabcentral/fileexchange/10590-fwhm/content/fwhm.m>.